Online Impedance Spectroscopy Characterization of PV Panels by Studying Resonant Behavior of Boost Converter

Xin Wang, Zhixue Zheng, Michel Aillerie, Alexandre de Bernardinis, Marie-Cécile Péra, Daniel Hissel

Online Impedance Spectroscopy Characterization of PV Panels by Studying Resonant Behavior of Boost Converter

Xin Wang*, Zhixue Zheng*, Michel Aillerie*, Alexandre De Bernardinis
Laboratoire Matériaux Optiques, Photonique et Systèmes (LMOPS)
Université de Lorraine, CentraleSupélec
F-57000 Metz, France
xin.wang@univ-lorraine.fr, zhixue.zheng@univ-lorraine.fr, michel.aillerie@univ-lorraine.fr, alexandre.de-bernardinis@univ-lorraine.fr

Marie-Cécile Péra, Daniel Hissel
Franche-comté Electronique Mécanique Thermique et Optique-sciences et Technologies (FEMTO-ST) Institute, FCLAB, CNRS
Université de Franche-comté
Belfort, France
marie-cecile.pera@univ-fcomte.fr, daniel.hissel@univ-fcomte.fr

***Abstract*—Impedance spectroscopy (IS) is a powerful in-operando characterization tool in the electrochemical domain which allows acquiring system internal impedances over a wide frequency range. Such information is valuable for understanding of the fundamental processes occurring within the system at different timescales. Compared with the specially designed workstations for IS implementation, the converter based IS is more advantageous in reducing the system cost and facilitating onboard applications, as no additional device is required. Considering the control simplicity and tracking rapidity, the open-loop control scheme for online IS implementation is initially studied and analyzed in this work. Due to the series connection of the inductor and the capacitor in the conventional boost converter, resonance can occur as the resonant frequency is usually covered by the wideband perturbation frequency. The resonance can cause the operating points to enter the nonlinear operating region of the target system and lead to invalid and distorted IS measurements. In this work, aiming at the photovoltaic (PV) panels, the influences of different system parameters, including parasitic resistances, converter passive components and steady-state output power, on the resonant behavior in open-loop control are systematically analyzed. Both simulation and experimental results are given to verify the proposed design guide.**

***Index Terms*—resonance, boost converter, impedance spectroscopy**

I. Introduction

The increasing demand for reducing greenhouse gas and increasing renewable sources adoption resulted in an increase of the installation of the photovoltaic (PV) systems, which play an important role in nowadays' microgrid applications [1]. Health monitoring is essential for detecting the occurring faults of the system, identifying its degradation states and ensuring the reliable operation of microgrids. Impedance spectroscopy (IS) is a well-recognized characterization tool which has received increasing attention in the health monitoring of different systems, such as fuel cells [2] [3], lithium batteries [4] [5] and more recently PV cells/panels [10]. IS measures the system internal impedances by injecting small perturbation current/voltage signals into the system over a wide frequency range and measuring the corresponding voltage/current response signals. As for PV applications in microgrid, IS is a promising diagnostic tool as no disconnection of PV panels from the microgrid is required, while a quasi-maximum output power of PV panels can be assured during the detection.

IS is commonly implemented based on a specially designed workstation which is generally high-cost, cumbersome and not practical for online applications. The converter based IS has been thus proposed in recent years in order to assure that the tested system operates under real operating conditions while unaffected by the measuring procedure [6]- [12]. Thus, it can be regarded as a real in-operando tool as it monitors the target system (not limited by an individual cell component) during operation and non-destructive. Meanwhile, the implementation cost can be much reduced as no additional device is required.

In the literature, there exists several ways for converter based IS implementation. According to the control loop scheme for perturbation signal injection, it can be divided into open-loop and closed-loop control. The open-loop control is relatively simple in design and has a rapid response time. In [6], an open-loop control of the duty cycle was applied in a dc/dc converter. A small perturbation ac signal was injected by directly modulating the duty cycle of the switch. However, the resonance caused by the series connection of the inductor and capacitor was ignored. Authors in [7] have observed the resonant behavior of their boost converter during IS measuring of two lithium-ion battery cells. An inner current feedback loop was added to make compensation. However, this paper

French national agency ANR project JCJC EREMITE (ANR-19-CE05-0008-01) and the Chinese Scholarship Council (CSC)

focused on the soft output voltage of the converter, which is only suitable for the system with constant input voltage. Authors in [8] has initially pointed out the resonant behavior of a boost converter during the IS characterisation of a single battery cell. They proposed directly a current-mode control loop for IS implementation without further focus on the open-loop control. In [9], the authors have mainly focused on the oscillations effect brought by IS on the common dc link in a hybrid fuel cell powertrain application. The resonance influence was equally ignored since a current control loop was utilized.

Authors in [10]- [12] have proposed online IS measuring methods for PV systems. However, the resonant behavior of the connected dc/dc converters was not spotted or ignored even for the open-loop control scheme. As analyzed in [13], to obtain rich internal information of PV panel, a wide frequency range is generally required. In the literature, the maximum injection frequency for PV panel can reach 100 kHz to acquire a complete Nyquist plot. When the frequency of the perturbation signal is extremely high, the closed-loop control method will be much limited by its bandwidth and the tracking speed. Compared with closed-loop control, open-loop control is more suitable for wideband perturbations due to its tracking rapidity. Therefore, this work focuses initially on the open-loop control based IS and a systematic analysis of the resonant behavior. The general validity conditions such as linearity, stability and causality are basically considered during the IS implementation.

In this paper, based on PV panel and a conventional boost converter, the influences of different system parameters, including parasitic resistances, converter parameters and steady-state output power, on the resonant behavior are analyzed. In section II, based on the state-space average model, the resonant frequency and corresponding small-signal duty-cycle to current transfer function are derived. The influences of different parameters on the resonance peak and frequency are further analyzed. The experimental verifications under different parameter configurations are given in section III, followed by a conclusions and perspectives in section IV.

II. Influence of Resonance Behavior on its Implementation

A. Resonant behavior of conventional boost converter

The topology of conventional boost converter is shown in Fig.1. The corresponding symbols and parameters are listed as follows: S-the input voltage source which can be a PV panel, V_{in} and i_L - the input voltage and current, L and r_L - the inductor and its parasitic resistance, T and Diode - the switch and diode, C and r_C - the dc bus capacitor and its parasitic resistance, v_o and R_L - the DC bus voltage and the load. When T is turned off and the boost converter operates with a given duty cycle D, the inductor L is in series with the bus capacitor C. For online IS implementation, a broadband ac perturbation signal is injected into the converter. In the open-loop control case, a small ac perturbation signal (from mHz to kHz) is directly superimposed to the steady-state

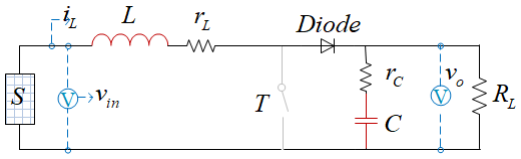

Fig. 1. Equivalent circuit of conventional boost converter when switch T is turned off

D. Consequently, the resonant frequency f_{res} can be easily covered by the broadband range, and the resonant behavior due to the L-C series connection can occur (the calculation of f_{res} will be given in section II.B).

During the occurrence of resonance, the overall equivalent resistance of the converter and the load is much reduced. The resulted perturbation current is large and can easily enter the nonlinear operating region. This violates the linear condition of valid IS measurements and significant distortion can be observed in the measured voltage and current signals. A more detailed analysis of the resonant behavior and the influences of different parameters on it are given in the following sections.

B. Analysis of resonant behavior based on state-space average model

State-space average model is a well-known technique to obtain an average, linearized model of switching converters. To analyze the resonance of the conventional boost converter during the injection of perturbation signals, the average model of boost converter in Fig.1 and can be expressed as:

when T is turned on:

$$\begin{cases} \dot{x} = A_1 x + B_1 v_{in} \\ v_o = C_1 x \end{cases} \tag{1}$$

when T is turned off:

$$\begin{cases} \dot{x} = A_2 x + B_2 v_{in} \\ v_o = C_2 x \end{cases} \tag{2}$$

where $x = [i_L v_c]^T$, and the $\dot{x}$ means its time-derivative. When the value of R_L and r_C satisfy: $R_L \gg r_C$, the parameters' arrays are specified as:

$$A_1 = \begin{bmatrix} -\frac{r_L}{L} & 0 \\ 0 & -\frac{1}{C \cdot R_L} \end{bmatrix}, B_1 = \begin{bmatrix} \frac{1}{L} \\ 0 \end{bmatrix},$$

$$A_2 = \begin{bmatrix} -\frac{r_L + r_C}{L} & -\frac{1}{L} \\ \frac{1}{C} & -\frac{1}{L \cdot R_L} \end{bmatrix}, B_2 = \begin{bmatrix} \frac{1}{L} \\ 0 \end{bmatrix},$$

$$C_1 = \begin{bmatrix} 0 & 1 \end{bmatrix}, C_2 = \begin{bmatrix} r_C & 1 \end{bmatrix}.$$

When boost converter operates in continuous-current mode (CCM) with duty cycle of switch - d, its overall state-space average model by summing both states can be written as:

$$\begin{cases} \dot{x} = [A_1 d + A_2(1-d)]x + [B_1 d + B_2(1-d)]v_{in} \\ v_o = [C_1 d + C_2(1-d)]x \end{cases} \tag{3}$$

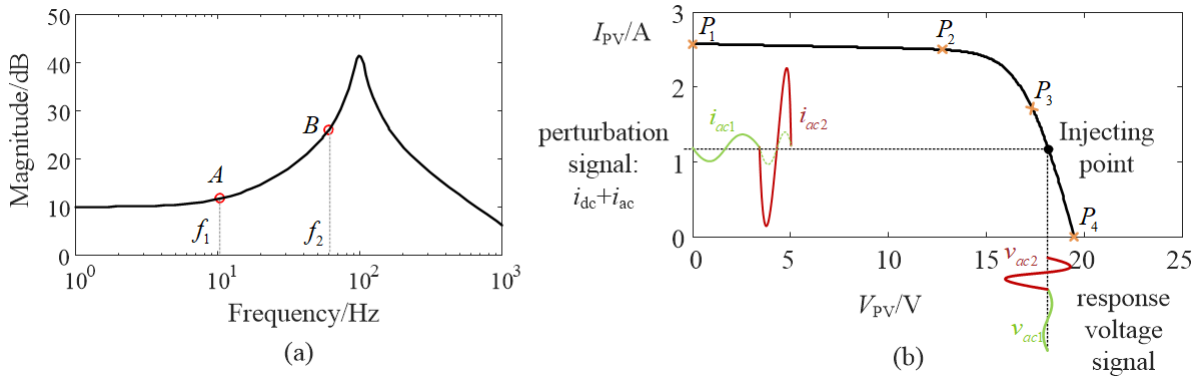

Fig. 2. (a) Magnitude of G_{i_L-d} (s) under different frequencies (b) Perturbation ac current signals and corresponding voltage signals

Considering a direct small-signal perturbation on duty cycle D in an open-loop control, the state-space model in (3) can be linearized around a steady-state D and all parameters are equal to a small-signal perturbations and a dc component, i.e., $d = D + \hat{d}$, $x = X + \hat{x}$, $v_{in} = V_{in} + \hat{v}_{in}$, $v_o = V_o + \hat{v}_o$. Therefore, the converter's response to the small-signal perturbation can be expressed as:

$$\begin{cases} \dot{\hat{x}} = [(A_1 - A_2)X + (B_1 - B_2)V_{in}]\hat{d} \\ \qquad + [A_1 D + A_2(1-D)]\hat{x} + [B_1 D + B_2(1-D)]\hat{v}_{in} \\ \hat{v}_o = [C_1 D + C_2(1-D)]\hat{x} + (C_1 - C_2)\hat{d}X \end{cases} \tag{4}$$

Where $\hat{d}$ is the small-signal perturbation on D, $\hat{x}$ and $\dot{\hat{x}}$ are the resulted perturbations on the state variable vector and its time derivative, $\hat{v_{in}}$ and $\hat{v_o}$ are the corresponding perturbations on the input voltage and dc bus voltage. In order to calculate the equivalent dynamic impedance of the boost converter and load (named as external impedance for simplicity), the transfer function of small-signal inductor current-to-input voltage $G_{v_{in}-i_L}$ by Laplace transform can be derived as follows:

$$\begin{aligned} G_{v_{in}-i_L}(s) &= \frac{\hat{v}_{in}}{\hat{i}_L}|_{\hat{d}=0} \\ &= sL + r_L + r_C(1-D) + \frac{R_L(1-D)^2}{1+sR_LC} \end{aligned} \tag{5}$$

Based on (5), the resonant frequency can be calculated:

$$f_{res} = \frac{1}{2\pi R_L C}\sqrt{\frac{R_L^2(1-D)^2C - L}{L}} \tag{6}$$

The smallest value of external impedance will be located at the resonant frequency where the corresponding phase value equals to zero. And the value of resonant frequency is influenced by the converter's parameters and the operating point.

C. Influence of different parameters on resonant behavior

To analyze the influence of perturbation of duty cycle on current signal of PV panel, the small-signal duty cycle-to-inductor current transfer function $G_{i_L-d}(s)$ by Laplace transform is calculated based on (4):

$$\begin{aligned} G_{i_L-d}(s) &= \frac{\hat{i}_L}{\hat{d}}|_{\hat{v}_{in}=0} \\ &\approx K_{sys}\cdot\frac{s/\omega_{z-sys}+1}{s^2/{\omega_{0-sys}}^2 + 2\zeta s/\omega_{0-sys}+1} \end{aligned} \tag{7}$$

where $\omega_{z-sys} = 2/R_LC$ and represents the frequency of zero; the gain of the system K_{sys} natural frequency ω_{0-sys} and damping ratio ζ are satisfied:

$$\begin{aligned} K_{sys} &= \frac{2V_{in}}{(1-D)^3R_L}, \\ \omega_{0-sys} &= (1-D)/\sqrt{LC}, \\ \zeta &= \frac{1/(R_LC) + (r_L + r_C(1-D))/L}{2\omega_{0-sys}} \end{aligned}$$

(7) shows that the perturbation current signal is influenced by input voltage V_{in}, the steady-state duty cycle D, the converter parameters including the inductor L and the bus capacitor C, the load R_L, and the corresponding parasitic resistances r_L and r_C.

Given an example of a system parameter set as: V_{in} = 16 V, D = 0.5, L = 2.5 mH, r_L = 0.1 Ω, C = 260 uF, r_C = 0.1 Ω, R_L = 80 Ω (more details of experimental setup are given in section III). The magnitude of changing with frequency is shown in Fig.2 (a). It can be observed that the amplitude of corresponding perturbation current signal first increases and then decreases. As shown in Fig.2 (b), the PV panel is a nonlinear system which consists of two quasi-linear regions (range P_1 – P_2 and P_3 – P_4) and one nonlinear region (range P_2 – P_3). To fulfill the linearity condition, the injecting point should be set in quasi-linear regions such as the indicated quasi-linear voltage region. For more details about the selection of injection regions and signal types, please refer to the authors' previous work [14]. As the perturbation frequency of small-signal duty cycle increases from f_1 to f_2, the corresponding ac current signal changes from i_{ac1} to i_{ac2} according to the transfer function as indicated in Fig.2 (a). The corresponding response voltage signal changes from v_{ac1} to v_{ac2} in Fig.2 (b). A nonlinear characteristic, e.g.,

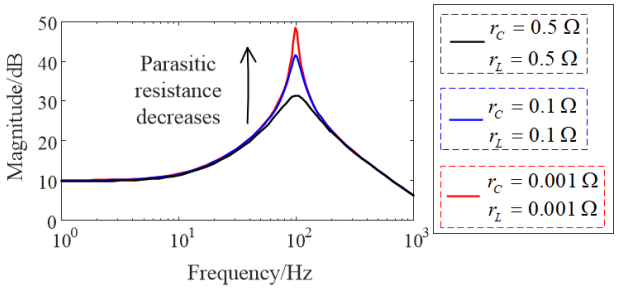

Fig. 3. Influence of parasitic resistances r_C, and r_L on the magnitude of $G_{i_L-d}(s)$

signal asymmetry or saturation, can be observed in v_{ac2}. As mentioned above, if this perturbation range covers the nonlinear operating region, the tested internal impedance of PV panel loses its validity since the linear condition is no longer satisfied.

Fig.4 illustrates the influence of parasitic resistances on the magnitude of transfer function $G_{i_L-d}(s)$. As can be observed, the parasitic parameters act as damping resistors. In the case of a quasi-ideal converter, the LC circuit is highly resonant with a significant peak, as illustrated by the red curve. However, increasing parasitic resistances can efficiently reduce the peak value and suppress the resonant behavior as illustrated by the black curve. Meanwhile, the resonance frequency is not influenced by the parasitic parameters which is coherent with (6).

The influence of passive components of the converter, i.e., L and C can be observed in Fig.4 (a) and (b). As illustrated, the resonant frequency is inversely proportional to both the inductor L and the bus capacitor C. The resonance peak is inversely proportional to the inductor L and proportional to the bus capacitor C. When the input voltage V_{in} is constant, both the duty cycle D and the load R_L determine the output power of the system. As shown in Fig.4 (c) and (d), compared with D, R_L rarely affects the resonant peak. As R_L increases or D increases, the peak of the resonance increases.

The perturbation current signal should have an appropriate amplitude to keep the operating points located in the quasi-linear region during the online IS implementation. Hence, to ensure the validity of the IS measurements in open-loop control, one major design guide for IS implementation is that a proper configuration of different parameters should be made to ensure the gain of $G_{i_L-d}(s)$ suppressed as much as possible, while meeting the basic constraints of converter harmonics and power losses.

III. EXPERIMENTAL VERIFICATION

A. Experimental platform

The experimental platform consisting of a PV panel, a boost converter, a resistive load, a controller, and corresponding sampling modules is shown Fig.5 (a). The dSPACE Microlabbox is used as the digital controller. The perturbation signal and corresponding responses are generated and collected by the controller. The current is measured by a current transducer IT 65-S ULTRSTAB with a high accuracy and wide frequency bandwidth. A half-bridge SiC power module (PEB 8024) with an integrated dc bus capacitor is utilised for power conversion. For the online test, the switching frequency is set as 20 kHz, and the frequency range of the perturbation signal is from 1 Hz to 1 kHz.

TABLE I
EXAMPLE STATE PARAMETERS

States	Parameters	Symbol	Value
State A	Inductance	L	2.5 mH
	Load	R_L	80 Ω
	Duty Cycle	D	**[0.3,0.4,0.5]**
	Input Voltage	V_{in}	[16.2,15.9,15.5] V
State B	Inductance	L	2.5 mH
	Load	R_L	**[60,80,96]** Ω
	Duty Cycle	D	0.4
	Input Voltage	V_{in}	[15.6,15.9,16.1] V
State C	**Inductance**	L	**[5,2.5,1.25]** mH
	Para-R	r_L	**[0.05,0.1,0.2]** Ω
	Load	R_L	80 Ω
	Duty Cycle	D	0.4
	Input Voltage	V_{in}	15.9 V

Para-R means Parasitic resistance

As shown in Fig.5(b), the amplitudes of voltage and current occur an increase due to resonance, during perturbation signal injecting. And if the there is no other changes in the control method and parameters of operating system, the operating point will enter non-linear region shown in Fig.5(c). The influence of the resonance on the test impedance will be analyzed in Section III.B.

B. Experimental results and analysis

As analyzed in Section II, the magnitude of $G_{i_L-d}(s)$ and its resonant frequency depend on their parasitic resistances, the passive components of the converter, and the steady-state output power of the system. Three parameter sets named state A, B and C are designed to study and verify the influences of different parameters. State A and B study the influence of output power with the same specifications of passive components. State C varies the passive components with a constant output power. As the dc bus capacitor is integrated inside the half-bridge module, only the inductor with its parasitic resistance is varied. Compared with the output power of the system, the power losses caused by the parasitic resistances are too small to be ignored.

The parameters of these three states are specified in Tab I. The internal impedance of PV panel under different operating parameter sets is measured and drawn in Fig.6 - Fig.8. According to the analysis, the resonance can cause an enlarged moving range of dynamic operating points during online perturbation. The operating points may easily enter the nonlinear operating region. As a result, the measured internal impedance is bigger than the actual one that measured in quasi-linear voltage region. To evaluate the influence of

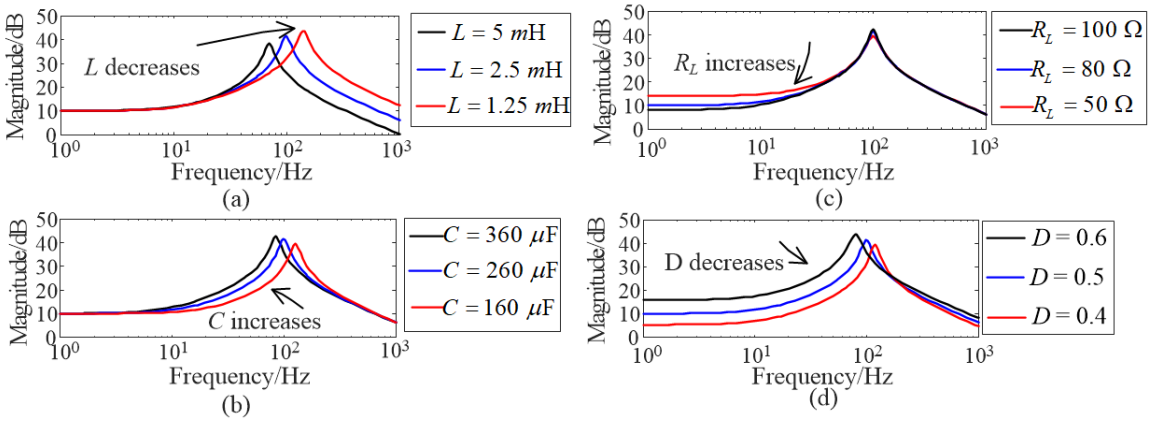

Fig. 4. Influence of parameters L, C, D and R_L on the magnitude of $G_{i_L-d}(s)$

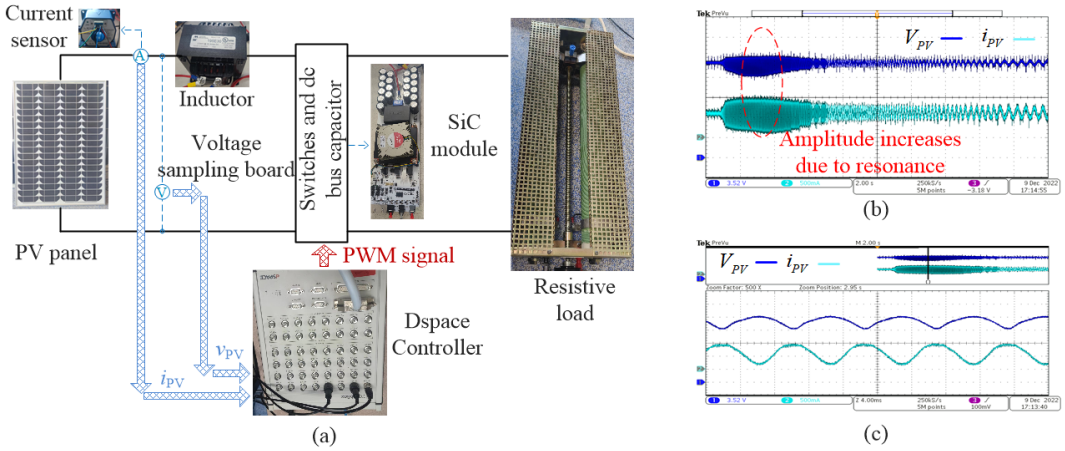

Fig. 5. Experimental platform for online IS implementation in the laboratory and experimental waveforms

resonant behavior on the measured PV internal impedance, the increasing rate of the internal impedance is defined as:

$$\eta_Z = (\Delta Z/|Z_1|) \cdot 100\% \tag{8}$$

where$\Delta Z = Z_{peak} - |Z_1|$, and $|Z_{peak}|$ and $|Z_1|$ represent the internal impedance at resonant frequency and at 1 Hz (the lowest perturbation frequency herein), respectively. A higher value of represents a bigger influence of the resonance and reflects a bigger amplitude of perturbation current signal at the resonant frequency (see section II.C).

In state A, R_L is kept constant. As D increases, V_{in} decreases, and the steady-state output power of PV panel increases. According to the analysis in Section II, as the duty cycle decreases, the value of amplitude of perturbation signal caused by resonance will decrease. And the experimental results in Fig.6 (b) show the same trend, where $I_{ac-maxd1,2,3}$ represent the maximum amplitude of perturbation signal at different duty cycle and $I_{ac-maxd3} > I_{ac-maxd2} > I_{ac-maxd3}$. In state B, D is set constant, while the value of R_L is changing. The waveforms of output current on this state is shown in Fig.7, the maximum amplitude of perturbation signal decreases with the decrease of the value of R_L ($I_{ac-maxR3} > I_{ac-maxR2} > I_{ac-maxR1}$), which is consistent with the analysis in Section II.

Based on equation (8), the values of η_Z can be calculated. In state A, $\eta_{Z_{3-D}} = 15.18\% > \eta_{Z_{2-D}} = 5.40\% \eta_{Z_{1-D}} = 2.31\%$(correspond to D = 0.3, 0.4, 0.5). In state B, $\eta_{Z_{1-r}} = 8.35\% > \eta_{Z_{2-R}} = 5.40\% > \eta_{Z_{3-R}} = 4.84\%$ (correspond to R_L = 60 Ω, 80 Ω, 96 Ω). Due to the resonance, the operating points enter in the non-linear region and there is an obvious error of the measured internal impedance. The closer the injecting point is to the non-linear region (in Fig.6 (a) and Fig. 7 (a), the smaller output voltage of PV panel), the greater influence caused by resonance, that means, the greater error of the measured internal impedance will be.

When the location of injecting point is the same, the larger value of resonant peak, the more significant error of the measured internal impedance as the experimental results of state C. In state$C$, there is a significant moving movement of the resonant frequency as changing the inductor's value as shown in Fig.8. As L increases, the resonant frequency decreases ($f_3 > f_2 > f_1$) which is consistent with Fig.4. The increasing rate η_z is much influenced by the parasitic resistances r_L. As L is closer to an ideal component (r_L decreases), the greater

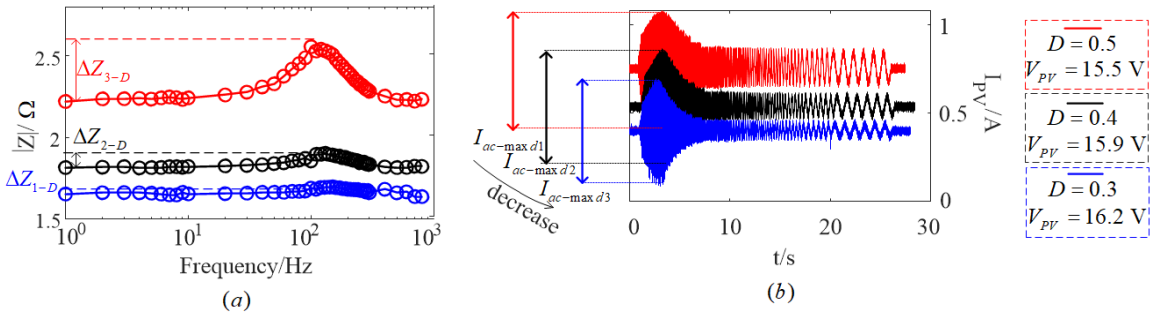

Fig. 6. Experimental waveforms under different duty cycles (a) internal impedance magnitude $|Z|$ (b) output current of PV panel

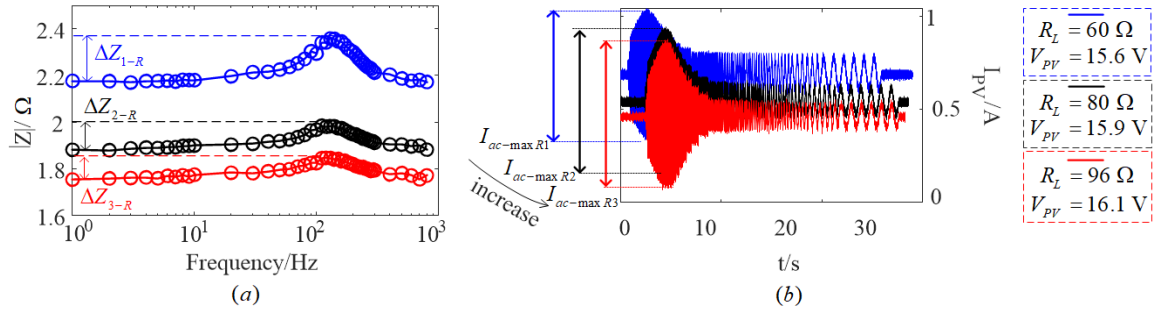

Fig. 7. Experimental waveforms under different loads (a) internal impedance magnitude $|Z|$ (b) output current of PV panel

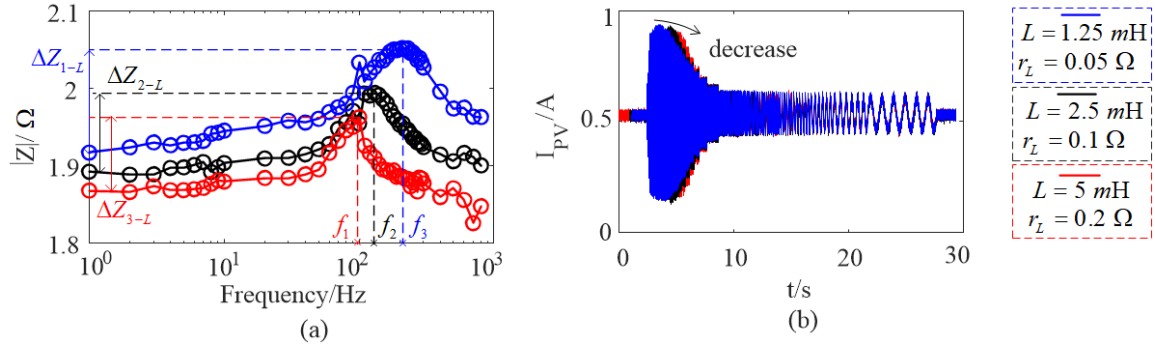

Fig. 8. Experimental waveforms under different inductors (a) internal impedance magnitude $|Z|$ (b) output current of PV panel

value of η_z can be observed: $\eta_{Z_{1-L}} = 7.07\% > \eta_{Z_{2-L}} = 5.40\% \eta_{Z_{3-L}} = 5.04\%$ ($\eta_{Z_{1-L}}, \eta_{Z_{2-L}}, \eta_{Z_{3-L}}$ correspond to r_L = 0.05 Ω, 0.1 Ω, 0.2 Ω).

To conclude, to reduce the resonance influence on the measured internal impedance of PV panel, it is preferable to choose the passive components with bigger parasitic resistances, and the injecting point smaller steady-state output power, under the premise of satisfying the system requirements of harmonics, power losses and efficiency. As shown in Fig.8 (b), the influence caused by resonance decreases both in the peak and the corresponding bandwidth by increasing L.

IV. Conclusion and Future Work

IS is an effective in-operando tool that can obtain real-time internal impedance information. Different to traditional IS implementation, which is generally based on a specially designed workstation, the way based on existing power converters such as boost converter can much facilitate the online health monitoring. The perturbation signals can be directly generated and injected by regulating the switches of the converter. However, as analyzed in this work, for the open-loop control of duty cycle, the boost converter shows an intrinsic resonant behavior during the wideband perturbation signal injection. This resonance can easily bring the operating points into the nonlinear operating region and lead to invalid IS measurements violating the linearity condition. The influences of different parameters, including the parasitic resistances r_C and r_L, the converter passive components L and C, and the steady-state output power (including the load resistance R_L and the duty cycle D), on the magnitude of small-signal duty cycle-to-inductor current transfer function $G_{i_L-d}(s)$, and the measured internal impedance of PV panel are consequently analyzed.

A guide of choosing the proper values of each parameter and the location of injecting point is proposed to reduce the resonance influence in the open-loop control. In future work, different solutions of suppressing the resonance influence will be further studied. And the design of a resonance compensator in the closed-loop control (current control or voltage control) while assuring the control bandwidth and tracking rapidity will be further analyzed. In addition, the influence of online IS implementation on the other interconnected converters and buses in microgrid applications will also be systematically evaluated and analyzed. Online health monitoring and fault diagnosis based on the obtained IS measurements will be also one of the focuses in the next steps.

ACKNOWLEDGMENT

The financial support of French national agency ANR project JCJC EREMITE (ANR-19-CE05-0008-01) and the Chinese Scholarship Council (CSC) are greatly acknowledged.

REFERENCES

[1] M. Shafique, X. Luo, and J. Zuo, "Photovoltaic-green roofs: A review of benefits, limitations, and trends," Solar Energy, vol. 202, no. October 2019, pp. 485–497, 2020.

[2] "A review of DC/DC converter-based electrochemical impedance spectroscopy for fuel cell electric vehicles," Renewable Energy, vol. 141, pp. 124–138, 2019.

[3] J. Z. Xiao-Zi Yuan, Chaojie Song, Haijiang Wang, Electrochemical Impedance Spectroscopy in PEM Fuel Cells. 2014.

[4] A. Kuperman, U. Levy, J. Goren, A. Zafransky, and A. Savernin, "Battery charger for electric vehicle traction battery switch station," IEEE Transactions on Industrial Electronics, vol. 60, no. 12, pp. 5391–5399, Dec. 2013.

[5] M. Crescentini et al., "Online EIS and Diagnostics on Lithium-Ion Batteries by Means of Low-Power Integrated Sensing and Parametric Modeling," IEEE Transactions on Instrumentation and Measurement, vol. 70, 2021.

[6] W. Huang and J. A. Qahouq, "An online battery impedance measurement method using DC-DC power converter control," IEEE Transactions on Industrial Electronics, vol. 61, no. 11, pp. 5987–5995, 2014.

[7] H. H. Abbasali and S. Jafarabadi Ashtiani, "Online Broadband Battery Impedance Spectroscopy Using Current-Mode Boost Converter," IEEE Transactions on Instrumentation and Measurement, vol. 71, pp. 1–8, 2022.

[8] J. A. A. Qahouq and Z. Xia, "Single-Perturbation-Cycle Online Battery Impedance Spectrum Measurement Method with Closed-Loop Control of Power Converter," IEEE Transactions on Industrial Electronics, vol. 64, no. 9, pp. 7019–7029, 2017.

[9] J. Shen and J. Wang, "Analysis of dc link oscillations in a hybrid fuel cell powertrain brought by in situ converter based electrochemical impedance spectroscopy," International Journal of Hydrogen Energy, vol. 45, no. 55, pp. 31080–31090, 2020.

[10] L. Shelembe and P. Barendse, "Online condition monitoring of Photovoltaic (PV) cells by implementing electrical impedance spectroscopy using a switch-mode DC-DC converter," ECCE 2020 - IEEE Energy Conversion Congress and Exposition, pp. 2136–2141, 2020.

[11] M. A. Varnosfaderani and D. Strickland, "Online Electrochemical Impedance Spectroscopy (EIS) estimation of a solar panel," Vacuum, vol. 139, pp. 185–195, 2017.

[12] O. I. Olayiwola and P. S. Barendse, "Power Electronic Implementation of Electrochemical Impedance Spectroscopy on Photovoltaic Modules," ECCE 2020 - IEEE Energy Conversion Congress and Exposition, pp. 3654–3661, 2020.

[13] E. Von Hauff, "Impedance Spectroscopy for Emerging Photovoltaics," Journal of Physical Chemistry C, vol. 123, no. 18, pp. 11329–11346, 2019.

[14] X. Wang, Z. Zheng, M. Aillerie et al., "Cooperative Control of Online Impedance Spectroscopy Monitoring Method and Maximum Power Point Tracking Method for Photovoltaic Panels," 2022 24th European Conference on Power Electronics and Applications (EPE'22 ECCE Europe), Hanover, Germany, 2022, pp. 01-10.